PROCEEDINGS OF SCIENCE

Modelling the multi-wavelength Non-thermal Emission of AR Sco

Louis du Plessis,[a,*] **Christo Venter,**[a] **Alice K. Harding**[b] **and Zorawar Wadiasingh**[c]

[a] *Centre for Space Research, North-West University, Private Bag X6001, Potchefstroom 2520, South Africa*
[b] *Theoretical Division, Los Alamos National Laboratory, Los Alamos, NM 58545, USA*
[c] *Astrophysics Science Division, NASA Goddard Space Flight Center, Greenbelt, MD 20771, USA*

E-mail: louisdp95@gmail.com

AR Sco is an intriguing binary system that contains both a white and red dwarf. The spin rate of the white dwarf has been observed to slow down with time, analogous to rotation-powered radio pulsars; it has thus been dubbed a "white dwarf pulsar". We previously fit the traditional radio pulsar rotating vector model to linearly polarized optical data from this source, constraining the system geometry and white dwarf mass. Next, using a much more extensive dataset from the South African Astronomical Observatory (SAAO) HIPPO Polarimeter on their 1.9-m telescope, we also explored the application of the same geometric model to the orbitally phase-resolved optical polarimetric data. The optical emission is thought to be due to non-thermal synchrotron radiation. We constrained the magnetic inclination angle and the observer angle at different orbital phases. Now, we have constructed a much more sophisticated emission model, solving the particle dynamics from first principles, including a generalized radiation reaction force, and implementing similar techniques to what were used in a pulsar emission code developed by A.K. Harding and collaborators to produce sky maps, light curves and spectra. We present our results of the particle pitch-angle evolution and Lorentz-factor evolution for different scenarios, as well as studying the impact of using generalised dynamical equations vs. a super-relativistic approximation only since our equations can also be applied to non-relativistic motion. Additionally, we investigate a magnetic mirror scenario, similar to that of Takata et al. (2017), and show the importance of not being constrained by assumptions of super-relativistic particles with small pitch angles. We also present some test cases that confirm the accuracy of our calculations. Finally, we discuss how we calculated the curvature and synchrotron radiation to obtain our emission maps, light curves and spectra as well as our future plans to calculate the phase-resolved polarisation properties of AR Sco.

High Energy Astrophysics in Southern Africa 2022 - HEASA2022
28 September - 1 October 2022
Brandfort, South Africa

*Speaker

PoS(HEASA2022)025

1. Introduction

AR Sco is a close white dwarf (WD) binary system observed to have pulsed non-thermal emission peaking in the optical range [1]. The autors inferred a spin period of 117s and an orbital period of 3.56h. Additionally, they found the M-dwarf companion to be located inside the magnetosphere of the WD. Extensive observations by [2] allowed them to constrain a spin-down rate for the WD. Observations by [3] found the optical emission to be highly linearly polarised (up to 40%), found a 180° polarisation angle swing and infered a B-field of $\sim 5 \times 10^8$G. The system also shows no indication of an accretion disk [1] as well as no accretion column [4]. In our previous work we fit a standard rotating vector model (RVM) to the polarisation angle data of AR Sco, constraining the magnetic inclination angle and observer angle [5]. This suggests the pulsed non-thermal emission is coming from inside the WD close to its magnetic poles. In a follow up paper we fitted the RVM to extensive polarisation angle data of AR Sco covering the orbital period of the system [6].

There have been various models proposed to reproduce the emission and polarisation signatures of AR Sco. None have been able to sufficiently produce light curves, spectra and polarisations curves over the spin and orbital phases. We thus aim to develop a general emission and polarisation model to reproduce the observations of AR Sco and similar sources. In this proceedings paper we discuss how we solved our particle dynamics in Section 2.1 and show our implementation of the radiation-reaction force(RRF) in Section 2.2. We show our results from reproducing the magnetic mirror model by 3 in Section 3 and make concluding remarks in Section 4.

2. Method

In this section we will discussed how we solved the particle dynamics with and without radiative losses for the particles as well as the accuracy tests we implemented.

2.1 Particle Dynamics

To find the particles' momentum and position at the next given time step we solved the Lorentz-force equation in cgs units:

$$\frac{d\mathbf{p}}{dt} = e\left(\mathbf{E} + \frac{c\mathbf{p}\times\mathbf{B}}{\sqrt{m^2c^4 + \mathbf{p}^2c^2}}\right) \tag{1}$$

where $\mathbf{p}$ is the particle momentum, e is the particle charge, $\mathbf{E}$ is the electric field, $\mathbf{B}$ is the magnetic field, m is the particle mass and c the speed of light in a vacuum. To obtain Equation (1), one uses $\mathbf{p} = \gamma m\mathbf{v}$ with $\gamma = \sqrt{m^2c^4 + \mathbf{p}^2c^2}/mc^2$, which comes from the particle energy $\gamma mc^2 = \sqrt{m^2c^4 + \mathbf{p}^2c^2}$. Equation (1) was written in terms of the particle's momentum to take into account relativistic aberrations. To solve this ordinary differential equation (ODE) we use higher order solvers with embedded lower order methods in the Runge-Kutta family of solvers. These implicit methods allows us to estimate a truncation error $T_{\rm err}$ with the absolute difference between the 2 order results. With $T_{\rm err}$ we can calculate an adaptive time step using [7]:

$$\Delta t_{n+1} = \Delta t_n \left(\frac{TOL}{T_{\rm err}}\right)^{-\frac{1}{(p+1)}}, \tag{2}$$

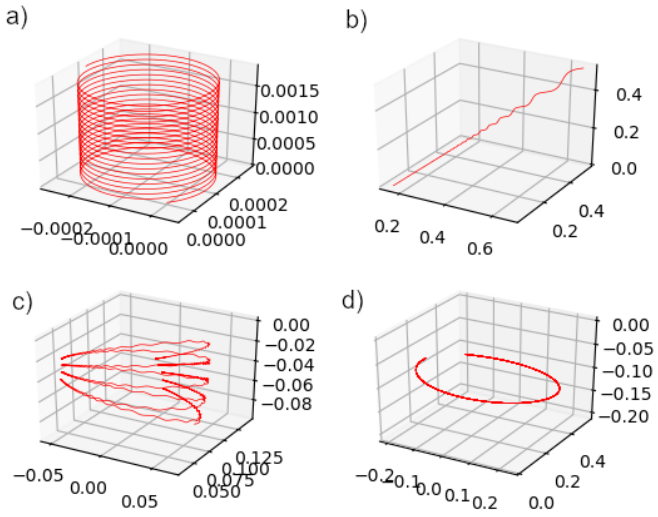

Figure 1: Panel a) is the particle trajectory for a constant B-field. b) is the trajectory for a changing B-field in a constant direction. c) is the trajectory for a static magnetic dipole field for a low B-field. d) is similar to c) but for a large B-field.

where Δt is the time step, TOL is the chosen tolerance for T_{err} and p is the order of the chosen numerical method. Soderlind [7] gives an equation for a limiting time step Δt_l for the maximum and minimum step size increase and decrease.

$$\Delta t_l = \Delta t_n \left[1 + \kappa arctan \left(\frac{\Delta t_{n+1} - \Delta t_n}{\kappa \Delta t_n} \right) \right], \tag{3}$$

with $\kappa \in [0.7, 2.0]$. We investigated various higher order numerical integrators and when balancing accuracy and runtime we chose the Dormand-Prince 8(7) [8] which was found to be about three times faster than the well known Runge-Kutta Fehlberg 4(5) scheme. Similar to other authors when talking about these schemes the accuracy order of the scheme is given after the scheme name followed by the error accuracy order in brackets.

To test the numerical schemes we use test scenarios with known particle trajectories, Lorentz-factors, gyro-radii and drift components. The first scenario is a constant B-field, second is a changing B-field, third is a low magnitude static dipole B-filed and fourth is a high magnitude static dipole B-field. The 3D trajectories for each scenario are illustrated in Figure 1. We show these test scenario results, benchmarks, elaborate on the particle dynamics and show the $E \times B$-drift scenarios in our upcoming paper Du Plessis et al (2023,in-prep).

2.2 Radiation-Reaction Force

To add a general radiation-reaction force (RRF) to our particle dynamics we use the following equation for Landau [9]:

$$\begin{aligned}\mathbf{f} =& \frac{2e^3\gamma}{3mc^3}\left\{\left(\frac{\partial}{\partial t}+\mathbf{v}\cdot\nabla\right)\mathbf{E}+\frac{1}{c}\mathbf{v}\times\left(\frac{\partial}{\partial t}+\mathbf{v}\cdot\nabla\right)\mathbf{H}\right\}\\ &+\frac{2e^4}{3m^2c^4}\left\{\mathbf{E}\times\mathbf{H}+\frac{1}{c}\mathbf{H}\times(\mathbf{H}\times\mathbf{v})+\frac{1}{c}\mathbf{E}\,(\mathbf{v}\cdot\mathbf{E})\right\}\\ &-\frac{2e^4\gamma^2}{3m^2c^5}\mathbf{v}\left\{\left(\mathbf{E}+\frac{1}{c}\mathbf{v}\times\mathbf{H}\right)^2-\frac{1}{c^2}\,(\mathbf{E}\cdot\mathbf{v})^2\right\}\end{aligned} \tag{4}$$

where $\mathbf{v}$ is the particle velocity and $\mathbf{H}$ is the external field thus $\mathbf{H}=\mathbf{B}$. The first term in Equation (4) is the contribution from the temporal and spacial changes in the field. This first term is very computationally expensive thus similar to [10] we evaluated the contribution of this first term and found it to be negligible. We also included the super relativistic form of Equation (4) from [9] to investigate the super-relativistic particle assumption and to save computation time for very large Lorentz factors. The x-component of the equation is given by

$$f_x = -\frac{2e^4\gamma^2}{3m^2c^4}\left\{\left(E_y-H_z\right)^2+\left(E_z+H_y^2\right)\right\}. \tag{5}$$

Since we have calculated the RRF we can calculate the energy radiated by the particle can be calculated using the following equation [11]

$$E_{\rm rad} = \int_{t_2}^{t_1}\mathbf{F}_{\rm rad}\cdot\mathbf{v}\cdot dt, \tag{6}$$

where $\mathbf{F}_{\rm rad}$ is the RRF. Using Equation(6) we can confirm if the code is self consistent by adding the particle energy with the energy radiated to get the total energy and compare this value to the initial particle energy. This allows us to see how accurate our calculations are and if our system is gaining or losing energy as is shown in Figure 2

Figure 2 shows an example chosen where the particle mirrors multiple times to illustrate the accuracy of our results. The figure shows how the particle radiates its energy at each magnetic mirror point represented by a sharp increase in the blue curve creating these step features. The total energy is found to be very close to the initial particle energy with $\sim 0.01\%$ energy loss. The accuracy can be increased by making the tolerance of the adaptive time step smaller at the cost of a longer runtime. We will show and discuss more of the RRF benchmarks and applications to the test scenarios in our upcoming paper Du Plessis et al (2023,in-prep).

3. Reproducing Takata et al

In this section we reproduce the magnetic mirror model proposed for AR Sco by [12] using our general equations as well as our super-relativistic equations.

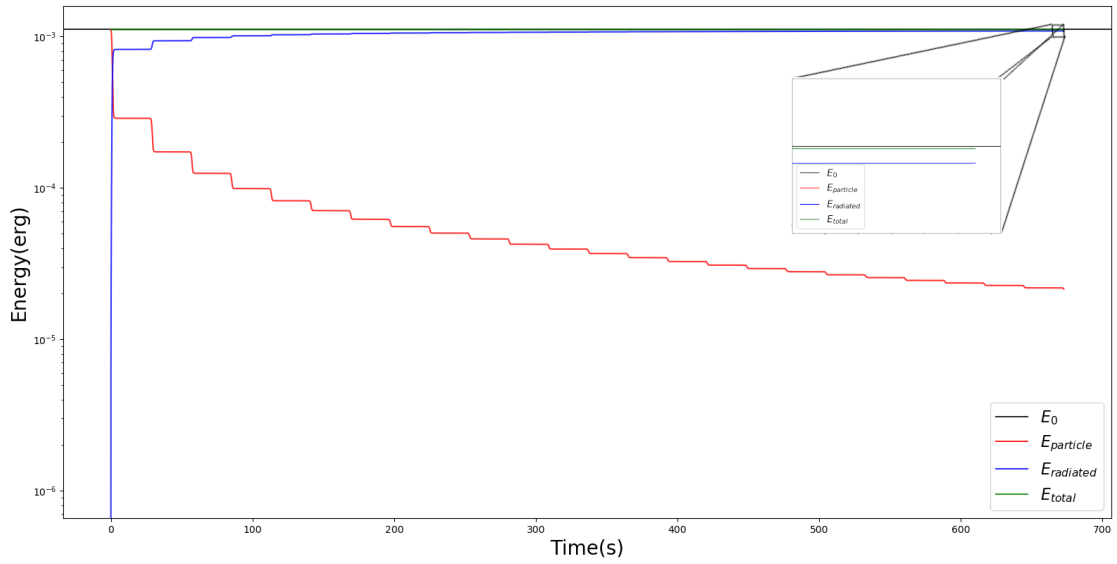

Figure 2: The energy radiated by a particle given by the blue curve and particle energy given by the red curve for a particle trapped in a magnetic dipole. The green curve is the sum of the red and blue curve with the black curve representing the initial particle energy.

In their paper [12] use the transport equations from [13] but written in terms of the second adiabatic invariant. The equations from [12] are given as:

$$\begin{aligned} \frac{d\gamma}{dt} &= -\frac{P_\perp^2}{t_s} \\ \frac{d}{dt}\left(\frac{P_\perp^2}{B}\right) &= -2\frac{B}{t_s\gamma}\left(\frac{P_\perp^2}{B}\right)^2, \end{aligned} \tag{7}$$

where $P_\perp$ is the momentum component perpendicular to the local B-field, γ is the Lorentz-factor, $t_s = 3m_e^3c^5/2e^4B^2$ and $P_\perp = \gamma\beta\sin\theta_p$. These equations assume that the particle is super relativistic and have small pitch angles. For the comparison scenario parameters they assume a static vacuum dipole B-field with zero magnetic inclination, a magnetic moment of $\mu_{WD} = 10^{35}\,\mathrm{G\,cm^3}$, $E = 0$ since the electric field is screened, $\gamma_0 = 50$ and a pitch angle of $\theta_p = \arcsin(0.1)$. We use their parameters to reproduce their results given in Figure 3. In Figure 3 the particle starts at the companion and heads toward the pole of the WD where it encounters a magnetic mirror. The particle radiates via synchrotron radiation as the particle then turns around due to the magnetic mirror and heads to the other pole of the WD. We found that our super-relativistic results mostly agree with that of [12] but our particle turns around at the magnetic mirror before their result. Our general results disagree largely with that of [12]. For our general results the particle bounces between multiple magnetic mirrors before the particle has lost the same amount of energy the particle losses at the first mirror in their results.

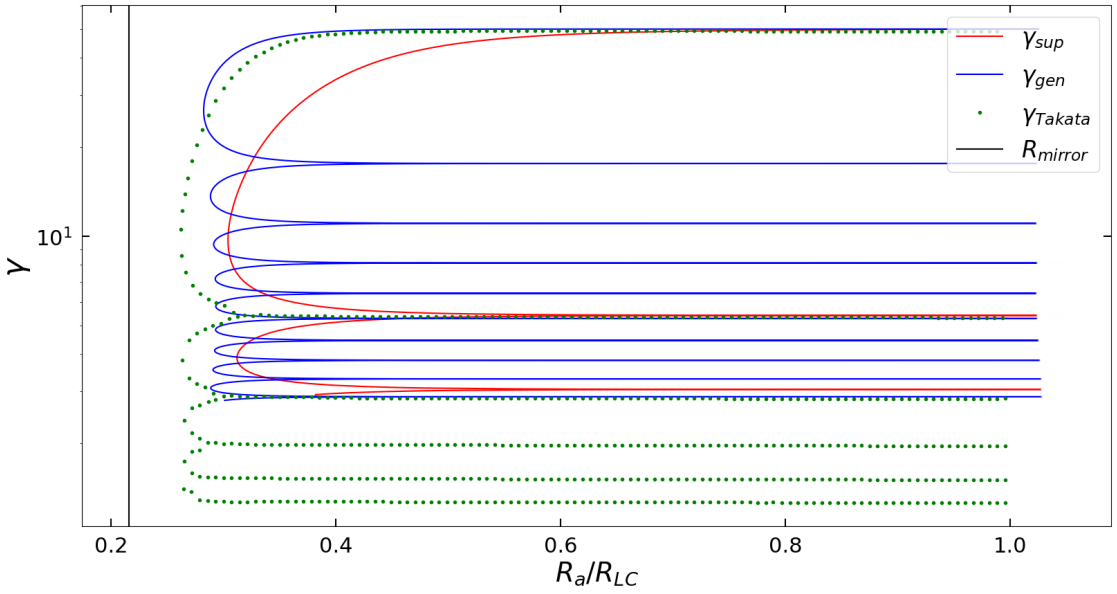

Figure 3: Lorentz-factor vs. the particle's radial distance normalised with the binary separation. The green dots are the digitised results from [12], the red curve is our results using Equation (5) and the blue curve using Equation(4). The black line represents the predicted magnetic mirror point from [12].

4. Conclusion

To conclude in Sections 2.1 and 2.2 we show how we solved the particle dynamics and introduced the RRF. We showed how we self consistently evaluate any energy gain or loss to numerical inaccuracy in the system obtaining accurate results without sacrificing more runtime. More in-depth results and benchmarks for the particle dynamics and test cases will be provided in our upcoming article as well as additional $E \times B$-cases and the RRF cases. In the magnetic mirror scenario proposed by [12] our results emphasise the importance of using the general particle dynamics instead of assuming the particles are super relativistic with small pitch angles. The super-relativistic assumption causes the particle to radiate much more at each mirror point affecting the particle dynamics differently. This leads to the emission being observed at different phases, different intensities, different mirror locations and different constraints on the particles trapped by the mirrors.

References

[1] T. R. Marsh, B. T. Gänsicke, S. Hümmerich, F.-J. Hambsch, K. Bernhard, C. Lloyd et al., *A radio-pulsing white dwarf binary star*, *Nature* **537** (2016) 374 [1607.08265].

[2] R. A. Stiller, C. Littlefield, P. Garnavich, C. Wood, F.-J. Hambsch and G. Myers, *High-Time-Resolution Photometry of AR Scorpii: Confirmation of the White Dwarf's Spin-Down*, *ArXiv e-prints* (2018) [1802.04323].

[3] D. A. H. Buckley, P. J. Meintjes, S. B. Potter, T. R. Marsh and B. T. Gänsicke, *Polarimetric evidence of a white dwarf pulsar in the binary system AR Scorpii*, *Nature Astronomy* **1** (2017) 0029 [1612.03185].

[4] J. Takata, C.-P. Hu, L. C. C. Lin, P. H. T. Tam, P. S. Pal, C. Y. Hui et al., *A Non-thermal Pulsed X-Ray Emission of AR Scorpii*, *Astrophys. J* **853** (2018) 106 [1712.06341].

[5] L. du Plessis, Z. Wadiasingh, C. Venter and A. K. Harding, *Constraining the Emission Geometry and Mass of the White Dwarf Pulsar AR Sco Using the Rotating Vector Model*, *Astrophys. J* **887** (2019) 44 [1910.07401].

[6] L. du Plessis, C. Venter, Z. Wadiasingh, A. K. Harding, D. A. H. Buckley, S. B. Potter et al., *Probing the non-thermal emission geometry of AR Sco via optical phase-resolved polarimetry*, *Monthly Notices of the Royal Astronomical Society* **510** (2021) 2998 [https://academic.oup.com/mnras/article-pdf/510/2/2998/42098443/stab3595.pdf].

[7] G. Söderlind and L. Wang, *Adaptive time-stepping and computational stability*, *Journal of Computational and Applied Mathematics* **185** (2006) 225.

[8] P. Prince and J. Dormand, *High order embedded runge-kutta formulae*, *Journal of Computational and Applied Mathematics* **7** (1981) 67.

[9] L. D. Landau, L. Landau and E. Lifshitz, *The Classical Theory of Fields: Volume 2*, vol. 2. Butterworth-Heinemann, 1975.

[10] B. Cerutti, A. A. Philippov and A. Spitkovsky, *Modelling high-energy pulsar light curves from first principles*, *Mon. Not. Roy. Astron. Soc.* **457** (2016) 2401 [1511.01785].

[11] J. D. Jackson, *Classical electrodynamics; 2nd ed.* Wiley, New York, NY, 1975.

[12] J. Takata, H. Yang and K. S. Cheng, *A Model for AR Scorpii: Emission from Relativistic Electrons Trapped by Closed Magnetic Field Lines of Magnetic White Dwarfs*, *Astrophys. J* **851** (2017) 143 [1712.03488].

[13] A. K. Harding, V. V. Usov and A. G. Muslimov, *High-Energy Emission from Millisecond Pulsars*, *Astrophys. J* **622** (2005) 531 [astro-ph/0411805].